

Vortex Chains and Vortex Jets in MoSi Microbridges

Volodymyr M. Bevz, Barbora Budinska, Sebastian Lamb-Camarena, Stanislava O. Shpilinska, Clemens Schmid, Mikhail Yu. Mikhailov, Wolfgang Lang, and Oleksandr V. Dobrovolskiy*

Superconducting bridges exhibit many properties of a Josephson junction, such as the electromagnetic radiation at overcritical currents $I > I_c$ and steps in the microwave-irradiated current–voltage (I – V) curves. These Josephson effects stem from the periodic motion of magnetic flux quanta (vortices) in the narrowest region of the bridge. According to the Aslamazov and Larkin (AL) theory, the I – V curve of such a constriction should exhibit voltage kinks each time the number of vortices in the 1D vortex chain is increased by one. However, in the presence of defects and fluctuations, the intervortex repulsion stipulates the formation of a 2D vortex jet, which goes beyond the 1D AL model. Here, by milling one or two slits across a MoSi thin strip, we make vortices to move in a vortex–jet or a vortex–chain fashion, respectively. Unexpectedly, for the strip with a vortex jet, we observe equidistant voltage kinks at transport currents $I \simeq 2I_c$ which are rather far from the assumption of $I \approx I_c$ in the AL model. At the moment, we have no explanation for this observation, tending to attribute it to fast relaxation processes in MoSi and looking forward for a comparison with other superconducting materials.

1. Introduction

Geometry-induced nonuniformities of the current streamlines are critical for superconducting single-photon detectors^[1] and crucially affect the penetration^[2] and patterns^[3] of magnetic flux quanta (Abrikosov vortices) in superconductors. In superconductor thin films, the vortex dynamics is 2D and it is controlled by the balance between various forces, among which

the vortex–current, vortex–defect, vortex–edge, and vortex–vortex interactions are most essential.^[4]


The effects of the current streamline bending on the vortex dynamics can be probed, for instance, via the artificial introduction of a single edge defect.^[5–7] An edge defect locally suppresses the energy barrier for the vortex entry^[8] and acts as a gate for fluxons which then cross the superconducting constriction under the action of the transport current.^[9] The repulsive interaction between vortices stipulates their arrangement in the form of a vortex jet,^[10] which has an apex at the defect and diverges toward the opposite edge of the constriction, see **Figure 1b**.

A defect at the opposite edge is expected to attract the vortices^[11] and—for the case of both defects placed on the same straight line—to promote the vortex–chain arrangement, see **Figure 1a**. For defects of the same strength, one will have a chain of

vortices and antivortices (vortices with the opposite direction of the circulating supercurrent), which will move from the defects toward the center of the constriction where they will annihilate.^[11–14] Distinct from this, if the edge barrier is suppressed by one of the defects considerably stronger, then one will deal with the dynamics of vortices of the same sign. Regardless of the asymmetry of the edge barrier suppression, such a constriction^[3] can be viewed as a wide ($w \gg \xi$, w : width; ξ :

V. M. Bevz
Physics Department
V. Karazin Kharkiv National University
61022 Kharkiv, Ukraine

B. Budinska, S. Lamb-Camarena, C. Schmid, W. Lang, O. V. Dobrovolskiy
Faculty of Physics
University of Vienna
1090 Vienna, Austria
E-mail: oleksandr.dobrovolskiy@univie.ac.at

 The ORCID identification number(s) for the author(s) of this article can be found under <https://doi.org/10.1002/pssr.202200513>.

© 2023 The Authors. physica status solidi (RRL) Rapid Research Letters published by Wiley-VCH GmbH. This is an open access article under the terms of the Creative Commons Attribution License, which permits use, distribution and reproduction in any medium, provided the original work is properly cited.

DOI: 10.1002/pssr.202200513

B. Budinska, S. Lamb-Camarena
Vienna Doctoral School in Physics
University of Vienna
1090 Vienna, Austria

S. O. Shpilinska
Faculty of Computer Sciences
University of Vienna
1090 Vienna, Austria

M. Yu. Mikhailov
B. Verkin Institute for Low Temperature Physics and Engineering of the National Academy of Sciences of Ukraine
61103 Kharkiv, Ukraine

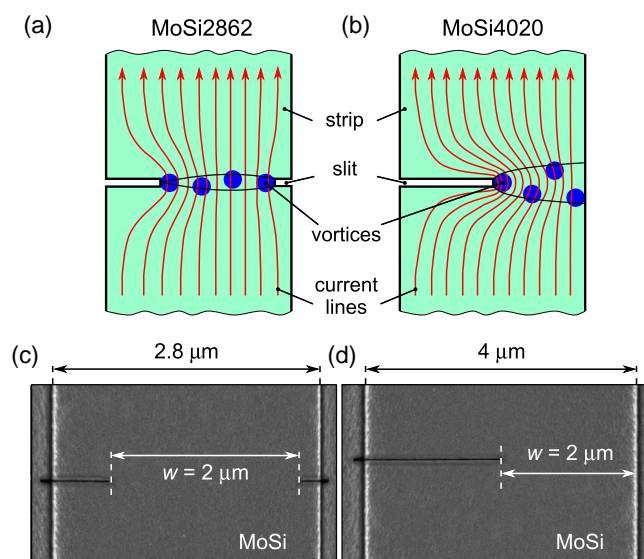


Figure 1. Sketches of the current streamlines bending in superconducting strips a) MoSi2862 with two slits and b) MoSi4020 with one slit. The vortex motion in the narrowest part of the bridge is assumed to occur in a 1D chain-like and a 2D jet-like fashion. c,d) Scanning electron microscopy images of the samples.

coherence length) Josephson junction, exhibiting such Josephson effects as the electromagnetic radiation at overcritical currents $I > I_c$ and steps in the microwave-irradiated I - V curves.^[15–22] These effects originate from the periodic motion of fluxons in the narrowest region of the bridge.

For a minor number of fluxons, the I - V curve of slitted superconducting thin strips will exhibit voltage kinks, which have recently been proposed as a hallmark for vortex counting and velocimetry.^[23] Within the framework of the AL model,^[12] there are several characteristic ranges of variation of the current, which differ in the number of vortices in the constriction. Qualitatively, the evolution of the vortex dynamics with increase of the current I can be described as follows.^[12] When I exceeds the critical value I_c by only a small amount, $I \approx I_c$, the time of formation of a vortex at an edge of the constriction is long and it is considerably greater than the time of the vortex motion across the constriction. Here, I_c corresponds to the vanish of the edge barrier and the entry of the first vortex into the constriction. With increase of I , the vortex nucleation time decreases and becomes shorter than the time of the vortex motion across the strip. The vortex-vortex repulsion makes difficult the nucleation of the next vortex which can then only be created when the preceding vortex has passed through almost the entire constriction. With a further increase of the current, this situation is repeated for a larger number of vortices. Expectedly, the addition of one vortex in the constriction becomes less appreciable when there are already many (n) vortices therein, $n \rightarrow (n + 1)$, that explains the kinks' smearing with increase of n .

Here, we compare the I - V curves for MoSi thin strips with one and two edge defects (slits), which exhibit voltage kinks as predicted by AL for wide Josephson junctions. By adjusting the strength of the edge barrier suppression via slit length variation, we realize the conditions for a 1D vortex chain (strip with

two slits, Figure 1a) and a 2D vortex jet (strip with one slit, Figure 1b). The geometrical parameters of the strips and the slits were chosen for the realization of one- to six-fluxon dynamics and the occurrence of one to six voltage kinks in the I - V curves. For both strips, we observe equidistant kink voltages. This finding agrees well with the AL model prediction for the strip with two slits for which the transport current $I \approx I_c$ and it is unexpected for the strip with one slit at transport currents $I \approx 2I_c$ which are rather far from the assumption $I \approx I_c$ in the AL model. Thus, our observation appeals for a comparative study of various superconducting materials.

2. Experimental Section

The strips were fabricated from a 15 nm-thick MoSi film on a Si/SiO₂ substrate. Details on the film fabrication and characterization were reported elsewhere.^[9] After the photolithography step, constrictions of 4 μm (sample MoSi4020) and 2.8 μm width (sample MoSi2862) were formed by a focused Ga-ion beam (FIB) milling. The sample names contained information on the bridge width and the slit lengths. Namely, in sample MoSi4020, the slit had dimensions 25 nm \times 2 μm (width \times length), resulting in the isthmus width $w = 2 \mu\text{m}$, see Figure 1b. In sample MoSi2862, two slits with the sizes 25 nm \times 0.6 μm and 25 nm \times 0.2 μm were milled in front of each other on the same straight line, see Figure 1a, resulting in the same isthmus width $w = 2 \mu\text{m}$. All slits were characterized by a partial suppression of superconductivity within a 5 nm-wide area around the slit. This suppression was caused by the Ga poisoning during the FIB milling. The 25 nm \times 2 μm slit in sample MoSi4020 was characterized by a very pronounced bending of the current streamlines at its apex, as shown in Figure 1b.

The samples were characterized by the resistivity $\rho_{8K} \approx 150 \mu\Omega \text{cm}$, critical temperature $T_c = 6.43 \text{ K}$, upper critical field $B_{c2}(0) \approx 10.2 \text{ T}$, electron diffusion coefficient $D \approx 0.5 \text{ cm}^2 \text{ s}^{-1}$, coherence length $\xi(0) = \sqrt{\hbar D / 1.76 k_B T_c} = 6 \text{ nm}$, penetration depth $\lambda(0) = 1.05 \cdot 10^{-3} \sqrt{\rho_{8K} / T_c} \approx 500 \text{ nm}$, and Pearl length $\Lambda(0) = 2\lambda^2(0) / d \approx 32 \mu\text{m}$. The $B_{c2}(0)$ value was deduced from the slope of the $B_{c2}(T)$ dependence according to the expression $B_{c2}(T) = B_{c2}(0) / 0.7 - (dB_{c2}/dT)T$.^[9] The dependence $B_{c2}(T)$ was obtained for nominally identical films patterned in the standard four-probe geometry, by using a $0.75\rho_{8K}$ resistivity criterion, in a series of out-of-plane magnetic fields.^[9] The condition $\xi \ll w < \Lambda$ justified the applicability of the AL theory,^[12] which ignored effects of the current-induced magnetic field variation on the superconducting properties. The I - V curves were acquired in the current-driven regime in zero magnetic field at $T = 4.2 \text{ K}$. The differential resistance data were obtained by differentiating the I - V curves with a running average over nine data points. The differential conductance data were additionally corrected by subtraction of the background.

3. Results and Discussion

Figure 2 and 3 present the I - V data for samples MoSi2862 and MoSi4020, respectively. For both samples, the I - V curves have a zero-voltage section (I) at low currents, an extended quasi-linear

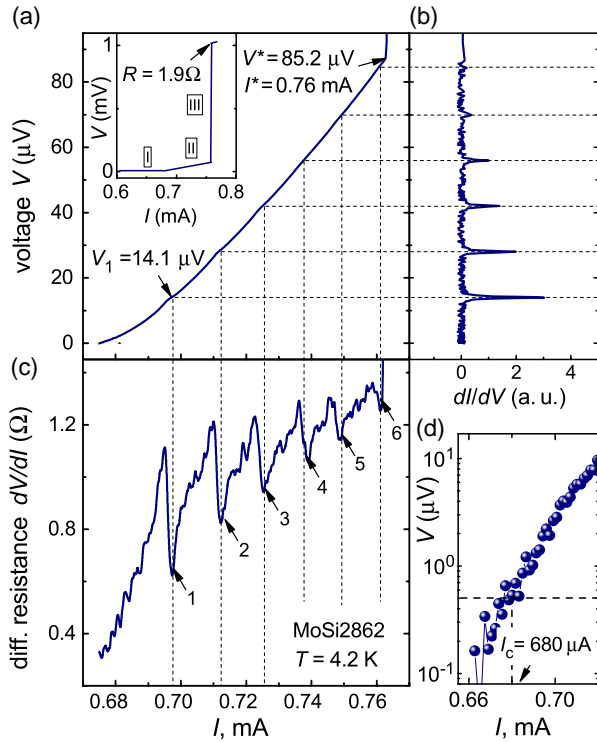


Figure 2. a) Voltage kinks in the current–voltage (I – V) curve of strip MoSi2862 at $T = 4.2$ K. Inset: The same I – V curve in a broader range of currents. b) Voltage versus differential conductance. c) Current dependence of the differential resistance. d) Initial part of the same I – V curve in the semi-logarithmic representation.

Ohmic branch (II) in the flux–flow regime, and an abrupt flux–flow instability (FFI)^[24,25] jump (III) to a higher resistive state (see the insets in Figure 2a and 3a). Both I – V curves exhibit voltage kinks in regime II. The kinks are nearly equidistant in voltage, occurring at integer multiples of the first-kink voltage $V_1^{\text{MoSi2862}} = 14.1 \mu\text{V}$ and $V_1^{\text{MoSi4020}} = 14.2 \mu\text{V}$. Up to six voltage kinks can already be recognized in the I – V curves, but even better so in the differential conductance and differential resistance curves shown in Figures 2b,c and 3b,c, respectively. From the rapid onset of the resistance at low voltages, we deduce the critical current $I_c^{\text{MoSi2862}} = 0.68 \text{ mA}$ and $I_c^{\text{MoSi4020}} = 0.53 \text{ mA}$ by using a 500 nV voltage criterion, see Figure 2d and 3d, respectively. The last voltage point before the FFI jump to the highly resistive state, $V_{\text{MoSi2862}}^* = 85.2 \mu\text{V}$ and $V_{\text{MoSi4020}}^* = 86 \mu\text{V}$, corresponds to an instability current of $I_{\text{MoSi2862}}^* \approx 0.76 \text{ mA} \approx I_c^{\text{MoSi2862}}$ and $I_{\text{MoSi4020}}^* \approx 1 \text{ mA} \approx 2 I_c^{\text{MoSi4020}}$.

At first glance, the I – V curves look qualitatively similar, exhibiting six kinks which are equidistant in voltage and having very close values of V^* at the FFI point. However, a detailed inspection of the I – V curves reveals their distinct features. First, the overall behavior of the differential resistance of strip MoSi2862 in Figure 2c has a tendency to increase while the I – V curve in Figure 2a exhibits a positive curvature up to the FFI point. In contrast, the overall behavior of the differential resistance of strip MoSi4020 in Figure 3c exhibits a flattening while the I – V curve in Figure 3a features a negative curvature

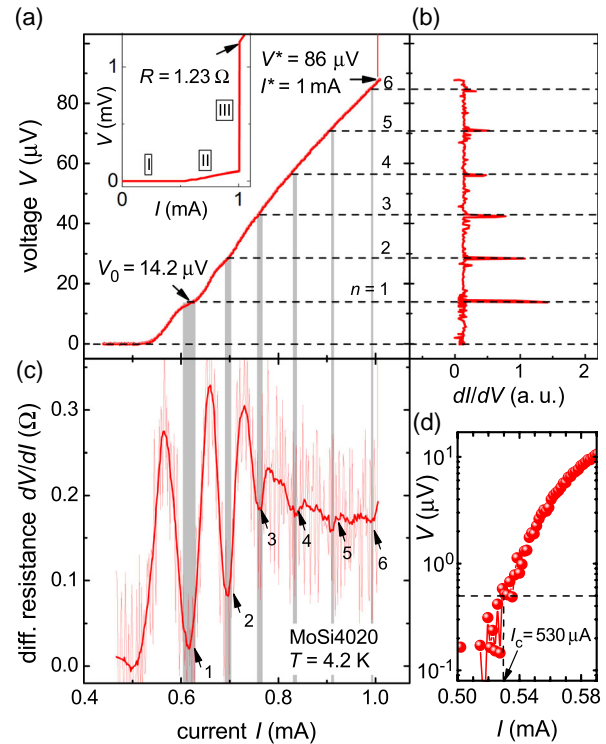


Figure 3. a) Voltage kinks in the I – V curve of strip MoSi4020 at $T = 4.2$ K. Inset: The same I – V curve in a broader range of currents. b) Voltage versus differential conductance. c) Current dependence of the differential resistance. The semitransparent red line corresponds to the differential resistance before averaging. d) Initial part of the same I – V curve in the semi-logarithmic representation.

close to the FFI point. Second, the minima in the differential resistance for strip MoSi2862 in Figure 2c look qualitatively similar. In contrast, the first three minima for strip MoSi4020 are very pronounced while the last three minima are hardly seen in Figure 3c. We tend to attribute this feature to some reconfiguration in the arrangement of vortices in strip MoSi4020. Overall, we have no explanation for this behavior as it implies that there appears some mechanism which impedes the motion of vortices at larger transport currents. As a result, the low-dissipative regime II is maintained up to larger currents for strip MoSi4020. Finally, the voltage kinks for strip MoSi4020 are sharper and look almost as steps in its I – V curve.

We note that the preservation of the low-dissipative state for strip MoSi4020 does not result in an appreciable increase of the instability voltage V^* and, hence, in an appreciable difference in the maximal vortex velocities in both samples, which can be estimated from the relation $v^* = wV^*/(n_v\Phi_0)$.^[23] Here, w is the isthmus width, n_v the number of vortices in the constriction, and Φ_0 the magnetic flux quantum. Substitution of the V^* values from the I – V curves in Figure 2a and 3a yields $v_{\text{MoSi2862}}^* \approx 13.73 \text{ km s}^{-1}$ and $v_{\text{MoSi4020}}^* \approx 13.86 \text{ km s}^{-1}$. The deduced v^* values are very close and agree well with the v^* values reported for MoSi from previous FFI studies on straight superconducting strips in the presence of small perpendicular magnetic fields. If one assumes that the FFI sets on when the

time of the vortex motion over the distance between two neighboring vortices becomes shorter than the time of healing of the order parameter wakes behind them, then the relaxation time can be estimated as $\tau_e = w/(v^* n_v)$, yielding $\tau_e^{\text{MoSi2862}} \approx 24.3$ ps and $\tau_e^{\text{MoSi4020}} \approx 24.0$ ps, which also agrees with the previous estimates.^[9,10] These estimates are made for the assumed vortex–river configuration (chain of vortices with depleted vortex cores) just before the FFI onset, as follows from the numerical solution of the time-dependent Ginzburg–Landau (TDGL) equation.^[10] The vortex river is formed because of the attraction of vortices to the wake with retarded recovery of the superconducting order parameter at high vortex velocities.^[10]

Within the framework of the AL model, the vortices are arranged in a 1D chain.^[12] In the presence of fluctuations and defects, however, a likely arrangement is a 2D vortex jet. The vortex jet shapes have been recently studied both analytically in the hydrodynamic approximation with respect to the density of vortices and their velocity field and numerically on the basis of TDGL simulations.^[10] Furthermore, vortex jets were experimentally observed in superconducting constrictions by scanning probe microscopy.^[3] Therefore, one may assume that one deals with a vortex jet in strip MoSi4020 while it is likely a vortex–chain arrangement in strip MoSi2862. In this sense, the double-slit geometry of strip MoSi2862 is closer to a wide Josephson junction with a chain of fluxons than the geometry of strip MoSi4020 in which the strong bending of current streamlines is likely to stipulate a vortex–chain to vortex–jet transition. The examination of this assumption should remain for vortex-imaging experiments and TDGL simulations. In particular, the recent TDGL equation modeling reveals an increase of the kink voltage height by about 15% with addition of one vortex for strips with shorter single slits and vortex–jet arrangements.^[23] While we have no explanation for the observation of the equidistant kink voltages for strip MoSi4020, we tend to attribute it to fast relaxation processes in MoSi and look forward for a comparison with other superconducting materials.

4. Conclusion and Outlook

We have studied the I – V curves for superconducting strips with one and two slits in which the vortex dynamics is realized in a vortex–jet or a vortex–chain fashion, respectively. For both geometries, we have observed up to six kinks in the I – V curves which are equidistant in voltage. Our central observation is that in contrast to the strip with two slits, whose resistive response at the transport current $I \approx I_c$ allows for treating its equidistant kink voltage spectrum within the framework of the AL model, this observation is unexpected for the strip with one slit at transport currents $I \approx 2I_c$ which are rather far from the assumption $I \approx I_c$ in the AL model. It would therefore be interesting to check whether the vortex–chain regime (or at least a decrease of the opening angle of the vortex jet) could be reproduced for strips with two slits placed on the same straight line in TDGL simulations. Similar to the convergence of a vortex–jet toward the opposite-edge defect, it would furthermore be interesting to check whether two edge defects somewhat displaced from the middle line of the constriction would allow for the stabilization of the vortex jet, impeding the onset of the FFI. Finally, an

interesting research direction would be to use the geometry-induced magnetic field nonuniformity in 3D superconducting membranes to control the transitions between vortex–chain and vortex–jet regimes.^[26] The understanding of the dynamics of vortices in such micro- and nano-architectures is required for the development of novel fluxonic devices for electromagnetic field sensing^[27] and information processing.^[28]

Acknowledgements

The authors are very grateful to Denis Yu. Vodolazov for numerous fruitful discussions. V.M.B. acknowledges the European Cooperation in Science and Technology (E-COST) for support via Grants No. E-COST-GRANT-CA16218-5759aa9b and No. E-COST-GRANT-CA16218-46e403c7. B.B. and S.L.C. acknowledge financial support by the Vienna Doctoral School in Physics (VDSP). S.L.C. thanks the Austrian Science Fund (FWF) for funding via Grant no. I 4889-N (CurviMag). S.O.S. acknowledges the OeAD (Austria's Agency for Education and Internationalisation) for support through the Ernst Mach Grant MPC-2022-03823, EM UKR/Batch II. M.Yu.M. acknowledges the Wolfgang Pauli Institute (WPI) Vienna for the scholarship within the framework of the Pauli Ukraine Project, the scholarship from the Krzysztof Skubiszewski Foundation, and the IEEE Magnetics Society for support via the STCU Project no. 9918. This research is funded in whole, or in part, by the Austrian Science Fund (FWF), Grant nos. I 6079-N (FluMag) and I 4865-N (FluxPin). Support by E-COST via COST Actions CA19108 (HiSCALE) and CA21144 (SuperQuMap) is gratefully acknowledged.

Conflict of Interest

The authors declare no conflict of interest.

Data Availability Statement

The data that support the findings of this study are available from the corresponding author upon reasonable request.

Keywords

Josephson junction, flux–flow instability, nanofabrication, superconductivity, vortex matter

Received: December 31, 2022

Revised: January 26, 2023

Published online:

- [1] J. R. Clem, K. K. Berggren, *Phys. Rev. B* **2011**, *84*, 174510.
- [2] O. A. Adami, D. Cerbu, D. Cabosart, M. Motta, J. Cuppens, W. A. Ortiz, V. V. Moshchalkov, B. Hackens, R. Delamare, J. Van de Vondel, A. V. Silhanek, *Appl. Phys. Lett.* **2013**, *102*, 052603.
- [3] L. Embon, Y. Anahory, Z. L. Jelic, E. O. Lachman, Y. Myasoedov, M. E. Huber, G. P. Mikitik, A. V. Silhanek, M. V. Milosevic, A. Gurevich, E. Zeldov, *Nat. Commun.* **2017**, *8*, 85.
- [4] E. H. Brandt, *Rep. Progr. Phys.* **1995**, *58*, 1465.
- [5] A. Aladyshkin, A. S. Mel'nikov, I. A. Shereshevsky, I. D. Tokman, *Physica C* **2001**, *361*, 67.
- [6] M. Friesen, A. Gurevich, *Phys. Rev. B* **2001**, *63*, 064521.
- [7] D. Y. Vodolazov, K. Ilin, M. Merker, M. Siegel, *Supercond. Sci. Technol.* **2015**, *29*, 025002.
- [8] G. P. Mikitik, *Phys. Rev. B* **2021**, *104*, 094526.

- [9] B. Budinská, B. Aichner, D. Y. Vodolazov, M. Y. Mikhailov, F. Porrati, M. Huth, A. Chumak, W. Lang, O. Dobrovolskiy, *Phys. Rev. Appl.* **2022**, 17, 034072.
- [10] A. I. Bezuglyj, V. A. Shklovskij, B. Budinská, B. Aichner, V. M. Bezv, M. Y. Mikhailov, D. Y. Vodolazov, W. Lang, O. V. Dobrovolskiy, *Phys. Rev. B* **2022**, 105, 214507.
- [11] L. I. Glazman, *Sov. J. Low Temp. Phys.* **1986**, 12, 389.
- [12] L. G. Aslamazov, A. I. Larkin, *Sov.-Phys. JETP* **1975**, 41, 381.
- [13] I. Y. Antonova, V. M. Zakosarenko, E. Il'ichev, V. I. Kuznetsov, V. A. Tulin, *JETP Lett.* **1991**, 54, 505.
- [14] T. Francavilla, R. Hein, *IEEE Trans. Magn.* **1991**, 27, 1039.
- [15] S. Shapiro, *Phys. Rev. Lett.* **1963**, 11, 80.
- [16] A. Barone, S. Pagano, in *Josephson Devices*, Springer, Cham **2000**.
- [17] A. G. Sivakov, A. M. Glukhov, A. N. Omelyanchouk, Y. Koval, P. Müller, A. V. Ustinov, *Phys. Rev. Lett.* **2003**, 91, 267001.
- [18] O. V. Dobrovolskiy, M. Huth, *Appl. Phys. Lett.* **2015**, 106, 142601.
- [19] U. Welp, K. Kadowaki, R. Kleiner, *Nat. Photon.* **2013**, 7, 702.
- [20] O. V. Dobrovolskiy, V. M. Bezv, M. Y. Mikhailov, O. I. Yuzepovich, V. A. Shklovskij, R. V. Vovk, M. I. Tsindlekht, R. Sachser, M. Huth, *Nat. Commun.* **2018**, 9, 4927.
- [21] T. J. Blom, T. W. Mechielsen, R. Fermin, M. B. S. Hesselberth, J. Aarts, K. Lahabi, *ACS Nano* **2021**, 15, 322.
- [22] S. S. Ustavschikov, M. Y. Levichev, I. Y. Pashenkin, N. S. Gusev, S. A. Gusev, D. Y. Vodolazov, *JETP Lett.* **2022**, 135, 226.
- [23] V. M. Bezv, M. Y. Mikhailov, B. Budinska, S. Lamb-Camarena, S. O. Shpilinska, A. V. Chumak, M. Urbanek, M. Arndt, W. Lang, O. V. Dobrovolskiy, *Phys. Rev. Appl.* **2023**, arXiv:2302.05100.
- [24] A. I. Larkin, Y. N. Ovchinnikov, *J. Exp. Theor. Phys.* **1975**, 41, 960.
- [25] A. I. Bezuglyj, V. A. Shklovskij, R. V. Vovk, V. M. Bezv, M. Huth, O. V. Dobrovolskiy, *Phys. Rev. B* **2019**, 99, 174518.
- [26] V. M. Fomin, R. O. Rezaev, O. V. Dobrovolskiy, *Sci. Rep.* **2022**, 12, 10069.
- [27] S. Lösch, A. Alfonso, O. V. Dobrovolskiy, R. Keil, V. Engemaier, S. Baunack, G. Li, O. G. Schmidt, D. Bürger, *ACS Nano* **2019**, 13, 2948.
- [28] V. M. Fomin, O. V. Dobrovolskiy, *Appl. Phys. Lett.* **2022**, 120, 090501.